



9th US National and 10th Canadian Conference on Earthquake  
Engineering: *Reaching Beyond Borders*

**toronto** july 25-29, 2010

9ième Conférence Nationale Américaine et 10ième Conférence  
Canadienne de Génie Parasismique: *Au delà des Frontières*

Conference Co-Sponsors  
Earthquake Engineering  
Research Institute

The Canadian Association for  
Earthquake Engineering

L'Association Canadienne du  
Génie Parasismique

## EFFECTS OF GROUND MOTION SCALING ON NONLINEAR HIGHER MODE BUILDING RESPONSE

Wood, R.L.<sup>1</sup> and Hutchinson, T.C.<sup>2</sup>

### ABSTRACT

Strategies for ground motion scaling are an active research topic in the earthquake engineering community. Considerations such as what amplitude, over what period range, and to what target spectrum are amongst the questions of practical importance. In this paper, the effect of various ground motion scaling approaches are explored using a suite of prototypical building models designed to respond nonlinearly under a design earthquake event. Using a site located in a densely populated region of the Los Angeles basin, a probabilistic seismic hazard analysis (PSHA) is conducted to estimate the magnitude and distance bins associated with a seismic hazard with a probability of exceedance of 10% in 50 years. Twenty-one recorded earthquake motions are selected based on compatible focal mechanisms, magnitude-distance pairs and local soil conditions. These motions are then scaled using three different strategies. The scaled motions are imposed on three code-designed reinforced concrete frame buildings of 8, 12 and 20 stories. Nonlinear response of the buildings is evaluated in terms of plasticity distribution, floor level acceleration and uncorrelated acceleration amplification ratio distributions; and interstory drift distributions. The most pronounced response variability associated with the scaling method is the extent of higher mode participation in the nonlinear demands.

### Introduction

Given the broad nature of earthquake motions, coupled with limited resources to analyze a particular problem, a natural question that arises in design is: How should a suite of motions be scaled to reasonably represent (in a conservative sense) the anticipated hazard at a site? Previous ground motion scaling methods have primarily focused on spectral acceleration amplitude scaling based on the fundamental period of the structure. For example, scaling the spectral acceleration at a single at the fundamental mode ( $T_1$ ) (e.g. Shone and Cornell, 1998). This has been extended in select applications to consider scaling across a period range, for example ASCE 7-05 requires that the average spectral acceleration of the suite of motions be greater or equal to the target spectral acceleration over the range of  $0.2T_1$  to  $1.5T_1$  when performing nonlinear time history analysis. It is noted that for single or short period sweep scaling approaches, the performance of systems with periods less than the fundamental mode or accounting for modes of vibration higher than the first mode can be misrepresented. Most nonstructural component systems (NCS) for example have primary modes of vibration with periods much smaller than the

<sup>1</sup> Graduate Research Assistant, University of California, San Diego, La Jolla, CA

<sup>2</sup> Associate Professor, University of California, San Diego, La Jolla, CA

building itself (less than 0.2 seconds). For these NCSs, the higher mode responses of the buildings are critical. Within the frequency range of say 5-20 Hz, reasonable transfer of the vibration energy is needed to predict the performance of the NCS. A scaling procedure based on the fundamental mode of a tall building can filter out the vibration energy associated with the NCSs. However as of yet, a consensus on the scaling for higher modes does not exist. A recently proposed method is the *Geometric Mean Method* by Huang et al. (2009). In this approach, a motion scale factor is selected to minimize the sum of the squared errors between the design (target) spectral acceleration and spectral acceleration ordinate of the selected record over a specified period range.

In this paper, an investigation is conducted to evaluate the sensitivity of the building's nonlinear time history response under three different scaling approaches. The scaling methods involve applying the geometric mean approach over the following period ranges: (i) between zero and four seconds (denoted *sweep*) and (ii) over the first two building periods (denoted *range*). A third method (iii) is considered for comparison where the scaling is performed only at the fundamental period of the structure (*fundamental*). Using a suite of ground motions selected to capture moment and distance pairs from a probabilistic seismic hazard, each ground motion record is scaled according to these three methods. Nonlinear time history analyses are cross compared and results reveal a weakness in the scaling approaches in the higher modes shown by divergent acceleration and interstory drift distributions.

### Site Location and Seismic Hazard

#### Site Location

The site selected for this study is located within a densely populated region of Southern California, in the city of Charter Oaks (longitude 117.856 W and latitude 34.102 N). The site was selected due to its high rate of seismic activity and proximity to a number of known fault zones. The site class was selected as C (dense soil), as defined by ASCE 7-05 (2005). Using the updated online National Seismic Hazard Maps (USGS, 2008), the spectral acceleration at short periods ( $S_s$ ) and at a period of one second ( $S_1$ ) were conservatively estimated as 2.01 g and 0.61 g, respectively, in the vicinity of the site. Using procedures of ASCE 7-05 (2005), a target design acceleration response spectrum, for a return period 475 years, was generated.

A PSHA of the site was undertaken to estimate the magnitude and source-to-site distance (M, R) bins associated with a seismic hazard with a probability of exceedance of 10% in 50 years. The hazard analysis was conducted using the USGS PSHA tools, which are based on the 2002 edition of the National Seismic Hazards Mapping Project models (USGS, 2002; Table 1). The deaggregation indicates that 98% of the hazard is associated with

Table 1. Deaggregation bin details (% hazard)

$M_w$	Source-to-Site Distance (km)			
	10	20	30	40
5.25	1.9	0.4		
5.50	1.2	0.3		
5.75	1.2	0.4		
6.00	2.6	1.1		
6.25	3.4	0.9	0.1	
6.50	9.0	2.7	0.2	
6.75	9.3	13.6	0.3	
7.00	18.6	16.4		
7.25	13.5	0.5		
7.50	1.0			
7.75				
8.00				0.7
8.25				0.6
<b>SUM</b>	<b>61.5</b>	<b>36.4</b>	<b>0.7</b>	<b>1.3</b>

sources within 12.4 miles or less, and approximately 60% of the hazard is associated with sources within 6.2 miles of the site.

The hazard deaggregation is used to guide the selection of ground motion records. The selection and scaling of ground motions is a broad and currently debated topic, however, based on the recommendations of ASCE 7-05 and those of Bommer and Acevedo (2004), it becomes evident that the selected ground motion records should conform to the following requirements:

- Strong motion records should be compatible with the tectonic regime anticipated at the site and of similar anticipated source mechanisms (i.e. strike-slip, reverse, or normal fault),
- Magnitude-distance (M, R) pairs of the selected records should be compatible with results of the deaggregation analysis from the probabilistic seismic hazard for the site of interest. With regard to magnitude selection, records were sought with magnitudes within 0.2 units of the target magnitude,
- The selected ground motion records should be compatible with the soil characteristics of the site of interest (namely site class C, with a shear wave velocity in the upper 100 feet ranging from 1200 to 2500 ft/s). Records at soft soil sites were excluded,
- Ground motion records should be obtained from strong motion instruments installed in the free field,

To obtain meaningful statistical results, a suite of 21 strong motion records with the aforementioned characteristics were selected from the PEER-NGA strong motion database (PEER, 2009). Of the selected motions, 11 were from the United States and Canada, two were from Italy and Japan, and one each were from Taiwan, USSR (Uzbekistan), Iran, Mexico and El Salvador. The records selected captured 94% of the total seismic hazard. The details on the ground motions are summarized in Table 2.

Table 2. Ground motions details and scale factors

Event	Date	Location	Focal Mechanism	Magnitude (Mw)	Distance (km)	Sweep	Range			Fundamental		
						All	20	12	8	20	12	8
Baja California	2-07-1987	Mexicali, Mexico	Strike-Slip	5.50	3.70	0.79	0.75	0.73	0.77	1.60	0.69	0.87
Cape Mendocino	4-25-1992	Cape Mendocino, CA, USA	Reverse	7.01	14.53	1.36	1.09	1.12	1.31	2.01	0.94	1.19
Cape Mendocino	4-25-1992	Cape Mendocino, CA, USA	Reverse	7.01	10.36	1.46	1.58	2.11	2.27	1.11	1.57	1.84
Chi Chi	9-25-1999	Taichung City, Taiwan	Reverse	6.30	11.52	1.89	1.57	1.67	1.94	3.20	1.62	1.27
Friuli	11-12-1999	Friuli, Italy	Reverse	6.50	14.97	1.82	2.25	1.89	1.74	4.39	2.36	2.26
Gazli	5-17-1976	Gazli, USSR	Reverse	6.80	12.82	1.03	1.05	1.35	1.07	0.97	1.14	1.47
Irpina	11-23-1980	Irpina, Italy	Normal	6.90	15.04	2.68	1.88	2.19	2.63	2.74	2.31	1.52
Kobe	1-16-1995	Kobe, Japan	Strike-Slip	6.90	7.08	1.17	1.17	0.97	1.00	1.44	2.09	1.45
Kobe	1-16-1995	Nishi-Akashi, Japan	Strike-Slip	6.90	8.70	0.91	1.73	1.41	0.89	1.38	2.01	2.08
Landers	6-28-1992	Lucerne, CA, USA	Strike-Slip	7.28	10.37	1.82	2.22	2.33	2.65	2.09	2.51	1.99
Loma Prieta	10-18-1989	San Jose, CA, USA	Reverse-Oblique	6.93	14.69	2.06	2.39	2.09	2.17	5.10	2.33	2.05
Loma Prieta	10-18-1989	Saratoga, CA, USA	Reverse-Oblique	6.93	9.31	1.23	0.83	0.99	1.43	1.15	0.75	0.89
Nahanni	12-23-1985	Nahanni, Canada	Reverse	6.76	6.52	1.38	1.00	1.15	1.51	2.86	1.01	0.90
Morgan Hill	4-24-1984	Morgan Hill, CA, USA	Strike-Slip	6.19	9.86	2.37	3.99	2.82	2.28	3.75	4.10	4.59
Northridge	1-17-1994	Castaic, CA, USA	Reverse	6.69	20.72	0.97	0.85	0.93	0.92	1.21	0.98	0.77
Northridge	1-17-1994	Los Angeles, CA, USA	Reverse	6.69	22.49	1.57	1.92	2.09	2.15	1.35	1.67	2.18
San Salvador	10-10-1986	San Salvador, El Salvador	Strike-Slip	5.80	6.99	1.16	0.80	0.95	1.20	0.79	0.83	0.67
San Fernando	2-09-1971	Castaic, CA, USA	Reverse	6.61	25.36	2.27	2.22	2.11	2.20	4.74	2.88	1.95
Superstition	11-24-1987	Superstition Mtn, CA, USA	Strike-Slip	6.54	7.50	0.87	1.09	0.93	1.01	2.81	1.63	0.86
Tabas	6-28-1991	Tabas, Iran	Reverse	7.35	2.05	0.55	0.57	0.56	0.59	0.56	0.86	0.59
Victoria	6-09-1980	Mexicali, Mexico	Strike-Slip	6.33	14.37	1.19	1.01	1.02	1.23	2.76	0.97	0.97
AVERAGE	-	-	-	6.66	11.85	1.45	1.52	1.50	1.57	2.29	1.68	1.54

## Scaling Methods

The motions were scaled using three different methods. Two methods involved variations of the Geometric Mean Method proposed by Huang et al. (2009). In this approach, the scale factor is selected to minimize the sum of the squared errors between the design (target) spectral acceleration and spectral acceleration ordinate of the selected record over a given period range. The scale factor  $a$  for an individual record is determined as follows:

$$a = \frac{\sum_{i=1}^n y_i \cdot y_i^t}{\sum_{i=1}^n y_i^2} \quad (1)$$

where,  $y_i$  = the spectral acceleration at period  $i$  and  $y_i^t$  = the target design spectral acceleration at period  $i$ . The geometric mean scaling approach was conducted in two ways: (i) the period range of zero to four seconds, termed “*sweep*” and (ii) period range corresponding to the first two building modes, termed “*range*”. The second method was used minimize the residuals over the 85% mass participation range. The (iii) third scaling method involved traditionally scaling only at the fundamental period, termed “*fundamental*”. Table 2 summarizes the resulting scale factors per motion considering each of the aforementioned methods. Note that on average the scale factors range from about 1.5 to 2.3.

## Building Design and Numerical Building Model Discretization

### Building Design

Three special moment resisting frame (SMRF) buildings intended to represent mid and high-rise buildings are used in the study (Figure 1). All buildings have the same footprint of 150 ft by 120 ft. The buildings are assumed to have five bays in each direction, with building dimensions as follows: longitudinal bay width of 30 ft, transverse bay width of 24 ft and story height of 12 ft. All buildings are assumed to have adequate foundation support, and therefore assumed fixed at their base. The design and analysis was conducted for the longitudinal direction of the prototype building. For the simplicity in analysis, only a single bay was analyzed. A live load of 50 psf was assumed, which is code-compliant for an office building (ICC, 2006). The dead load included, in addition to the self weight of the members, and a 10” thick two-way floor slab, a superimposed dead load of 20 psf. Conventional reinforced concrete was used for the design with a 28-day unconfined compressive strength of 5 ksi for the beams and between 5-10 ksi for the columns. The weight of the concrete was assumed to be 150 pcf. Grade 60 reinforcing steel, with a design yield tensile strength of 60 ksi was used throughout.

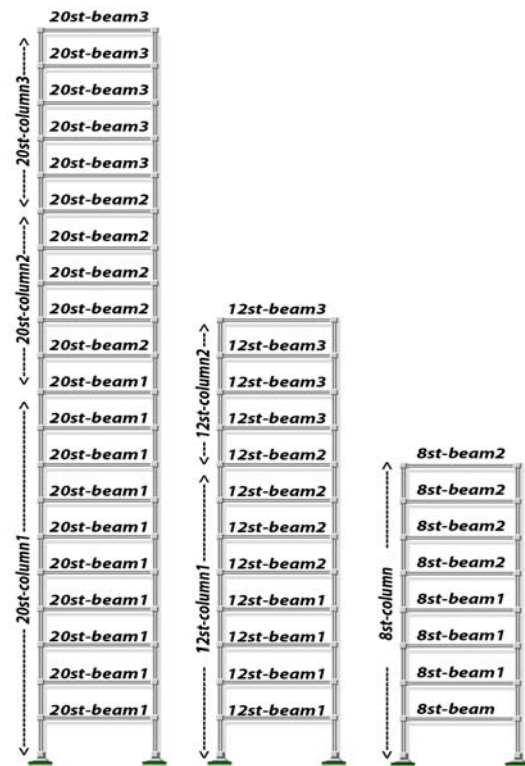


Figure 1. SMRF Building Designs  
(Note base of model fixed, and bottom of columns fixed)

Design was governed by IBC (ICC, 2006) and ACI 318-08 (ACI, 2008). The IBC 2006 design code provided estimates of the base shear, code-based period estimates and lateral force distribution, while ACI 318-08 was utilized for the general concrete design and detailing, with particular notice to Chapter 21. In the frame designs, strong column-weak beam philosophy was adopted, i.e. the sum of the moment capacity at the columns was designed to be at least 20% greater than the sum of the moment capacity at the beams. All of

Table 3. Building component details

Element	b (in)	h (in)	$f'_c$ (ksi)	Long. Reinf.	$\rho_l$ (%)	Conf.
8st-beam1	30	30	5	12 - #9s	1.34	#5 @ 5.5"
8st-beam2	26	30	5	10 - #9s	1.28	#5 @ 6.0"
8st-column	32	32	6	20 - #10s	2.67	#5 @ 4.0"
12st-beam1	30	30	5	12 - #9s	1.34	#5 @ 5.5"
12st-beam2	28	30	5	11 - #9s	1.10	#5 @ 5.5"
12st-beam3	24	28	5	9 - #9s	1.28	#5 @ 6.0"
12st-column1	32	32	8	20 - #10s	2.48	#5 @ 3.0"
12st-column2	32	32	8	16 - #10s	1.98	#5 @ 3.0"
20st-beam1	32	32	5	13 - #9s	1.27	#5 @ 5.0"
20st-beam2	30	30	5	12 - #9s	1.34	#5 @ 5.5"
20st-beam3	24	28	5	9 - #9s	1.28	#5 @ 6.0"
20st-column1	36	36	10	24 - #10s	2.35	#5 @ 3.0"
20st-column2	34	34	10	20 - #10s	2.20	#5 @ 3.0"
20st-column3	32	32	10	16 - #10s	1.98	#5 @ 3.0"

the SMRF buildings designed were governed by seismic loading. In the detailing of the beams and columns, the reinforcing steel was chosen to be in one layer for simplicity and double leg #4 stirrups were selected for shear reinforcement. The confinement spacing resulted in shear reinforcement providing a minimum lateral pressure of 9% of the target  $f'_c$  (Englekirk, 2003) within the assumed plastic hinge zone. Beams are assumed to be detailed symmetrically, i.e. compression reinforcement equal to the tension reinforcement. Columns are detailed with a single longitudinal reinforcement layer on each side for simplicity. Details of the building component designs are summarized in Table 3. The range of longitudinal reinforcing steel ratios  $\rho_l$  for the columns and beams is 1.1 – 2.7%. Additional building design details can found in Wood et al. (2009).

### Numerical Building Discretization

Numerical modeling of the prototypical buildings was conducted in the OpenSees (2008) platform. Two-dimensional model discretizations were developed assuming lumped masses and equivalent nodal loads. To account for large deformations, the corotational geometric transformation was used. Damping for the building models was set at 5% of critical, mass and stiffness proportional Rayleigh damping specified in the first two modes.

The building models were discretized using only one type of element, namely the *BeamWithHinges* element developed by Scott and Fenves (2006). This element was selected as it can be integrated with nonlinear fiber sectional discretization and has demonstrated good performance for members anticipated to undergo nonlinearity as well as softening or degradation (Scott and Fenves, 2006). The *BeamWithHinges* element also eliminates the nonobjective curvature response due to its sensitivity to the number of integration points (Coleman and Spacone, 2001). The element is developed as a force-based, lumped plasticity, zero-volume line element with two different sections, namely, a fiber section at each end, which represents the plastic hinge over a discrete length  $l_p$  - estimated using the Paulay and Priestley (1992) model - and an interior linear elastic section. In the development of the fiber section in the end regions, two material models were defined. Namely, the linear tension strength concrete (*concrete02*) and the Menegotto-Pinto model (*steel02*), for the reinforcing steel. The effects of confinement were accounted for using the model of Mander et al. (1988).

## Building Response and Discussion

### Eigenvalue Analysis

To determine the building dynamic characteristics, an eigenvalue analysis is carried out for all buildings models. Results from these analyses, in terms of the modal periods of vibration and modal mass participation estimates are shown in Table 4. The range of fundamental building periods is 0.89 seconds for the eight story SMRF to 2.07 seconds for the 20 story SMRF, with greater than 85% of the mass participating in the first two modes of vibration.

Table 4. Building eigenvalue analysis

Building	Period (sec)			
	1st	2nd	3rd	4th
<b>8 story</b>	0.89	0.29	0.15	0.1
<b>12 story</b>	1.33	0.45	0.24	0.16
<b>20 story</b>	2.07	0.71	0.39	0.26
Building	Mass Participation (%)			
	1st	2nd	3rd	4th
<b>8 story</b>	76.8	12.2	4.1	2.7
<b>12 story</b>	75.3	11.4	4.6	2.3
<b>20 story</b>	72.8	12.1	4.1	2.5

### Maximum Acceleration Distribution

Acceleration responses of the buildings in aggregate maximum floor level acceleration distributions are developed (Figure 2). The maximum acceleration distribution is calculated as the average of the maximum of the absolute value acceleration at each floor level obtained from each record. Plots are shown as a function normalized height ( $h^*=h_i/H$ ; where  $h_i$  = height of floor  $i$  and  $H$  = overall building height). At  $h^*=0$  the maximum acceleration is the peak ground acceleration. Note that the distribution of maximum acceleration does not follow a linear trend, but rather is linear at the lower floors (shear-like mode) and parabolic (bending-like mode) at the upper floors. Such a distribution indicates higher mode effects influence the nonlinear time history response. Considering the three different motion scaling methods, the amplitude of maximum acceleration varied most notably in the 20-story building. In the 20-story building, sweep scaling resulted in a maximum acceleration of approximately 1.5 g at the roof level, while fundamental scaling experienced nearly 2g at both the roof level and the 6<sup>th</sup> floor. For all buildings considered, the fundamental scaling approach resulted in the largest maximum floor level accelerations, though for the 8-story building these maxima are nearly identical to those of the range method. The dispersion in results for the different methods becomes larger with increasing building height.

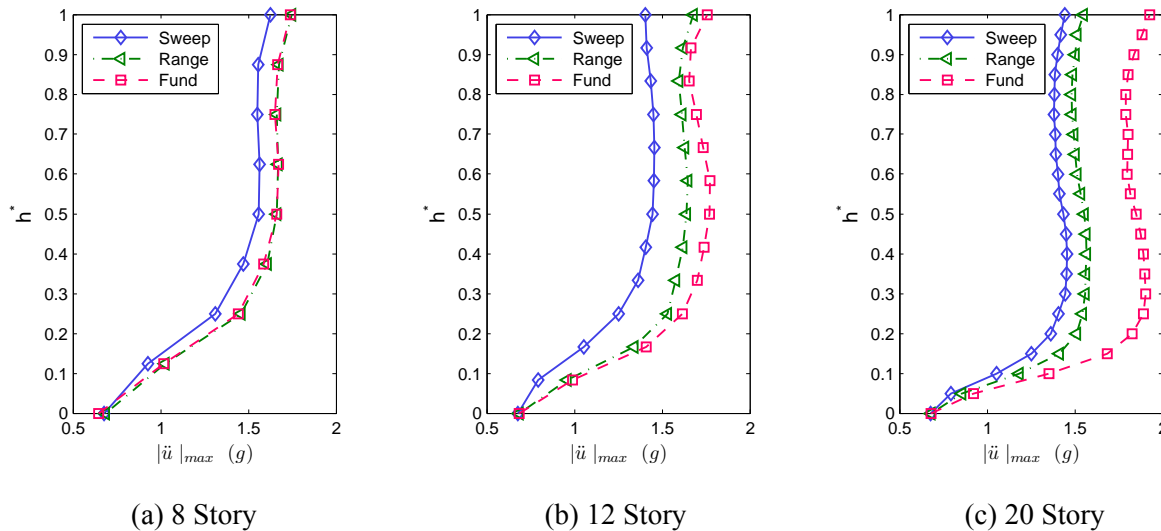


Figure 2. Maximum absolute floor acceleration by building type

## Acceleration Amplification Ratio Distribution

It is instructive to evaluate the correlation between maximum input acceleration and maximum floor acceleration. This comparison is often termed an uncorrelated acceleration amplification ratio i.e.:

$$\Omega_i = \frac{\max(|\ddot{u}_i|)}{PGA} \quad (2)$$

where  $\ddot{u}_i$  = the acceleration response of floor level  $i$  and  $PGA$  = the peak ground acceleration. This relationship is uncorrelated in the sense that the maximum floor level acceleration may not necessarily occur simultaneously with the peak ground acceleration. The average uncorrelated acceleration amplification ratio distributions (by record) are shown in Figure 3. This figure shows the uncorrelated acceleration amplification ratio distributions compared with the linear code-based suggestion of IBC (ICC 2006). As in the average acceleration plot; these structures demonstrate significant influence of higher modes. As a result of these higher mode effects, the prescribed code values underestimate the acceleration amplification ratio in the lower most floors for taller buildings, while conservatively overestimating amplifications in the upper most floors. The code prescribed values severely under-estimate the amplification experienced in the 20-story building for the fundamental scaling approach. The scaling method adopted affects the magnitude of the response and not the overall shape. The fundamental scaling approach indicates the largest acceleration amplification, particularly for the taller, 12 and 20-story buildings.

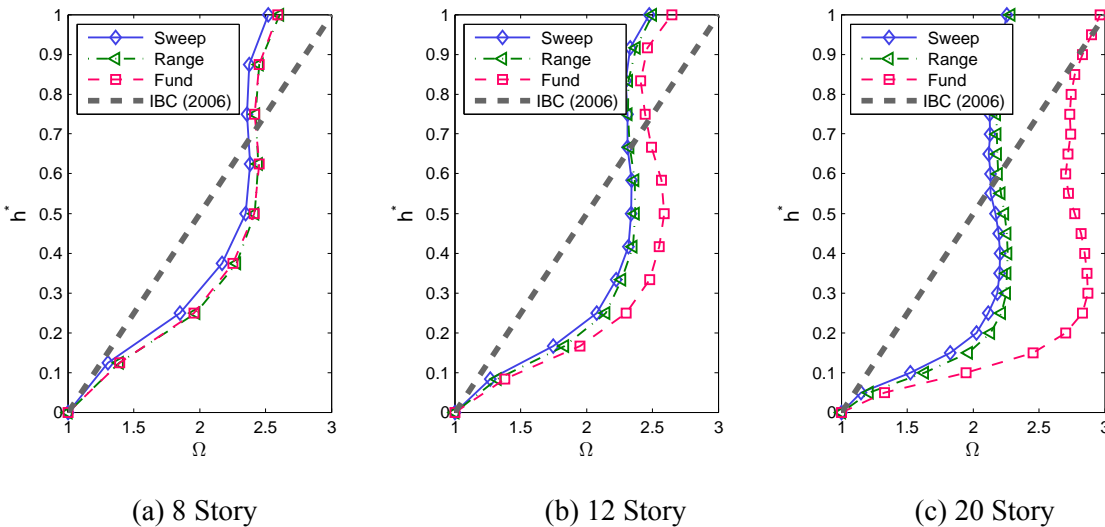


Figure 3. Average uncorrelated acceleration amplification factor  $\Omega$  by building type

## Interstory Drift Distribution

To characterize the deformation demand distribution within the building, the maximum interstory drift ratio is presented as a function of the normalized height  $h^*$  in Figure 4. In like fashion, the distribution demonstrates higher mode effects, as the shape is parabolic in nature, and the dispersion amongst results increases with increasing building height. For the 8 and 12-story buildings, the largest interstory drift is observed at approximately 40% of the building height, however for the 20-story the largest interstory drift demands are in the upper stories of the building, in this case on average at 85% of the height of the building. The scaling method

primarily controls the magnitude, as the shapes are similar. For the 12 and 20-story buildings, the fundamental scaling method results in the largest interstory drift demands. In contrast, the largest interstory drift demands in the 8-story building were observed using motions scaled with the range method.

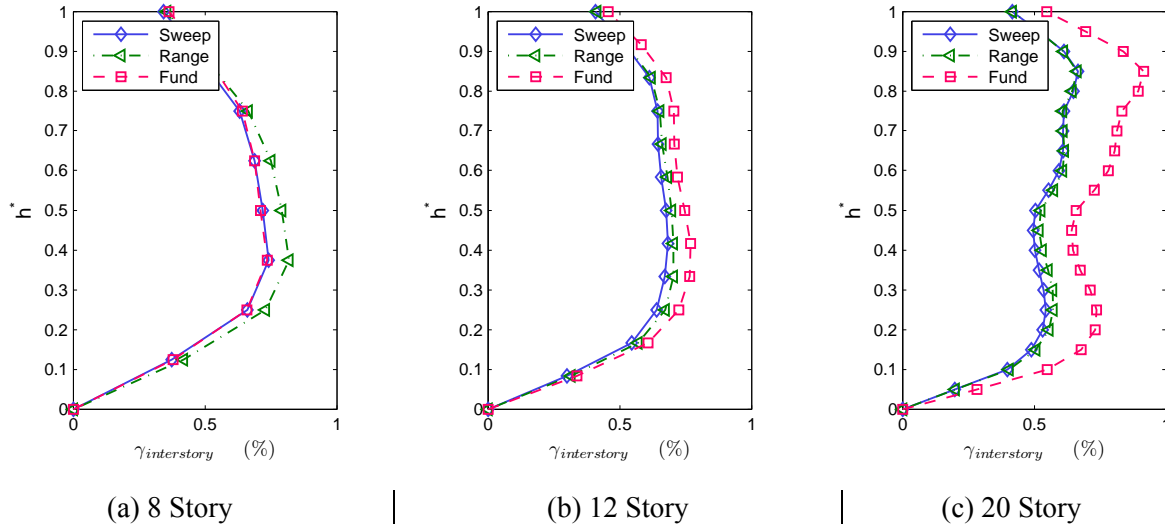


Figure 4. Average interstory drift ratio profiles by building type

### Plasticity Distribution

Curvature time histories provide an indication of the extent of plasticity the buildings experience during an earthquake excitation. To render these results graphically, plasticity distribution diagrams are developed, where maximum plastic rotation and curvature ductility values are reported (Figure 5). These plasticity distribution diagrams show a normalized bubble size at the locations where plasticity occurred. For the 8-story building, only minimal differences exist when comparing results using the three different scaling methods, however for the 12 and 20 stories differences are noted. Most notably, higher mode effects, which more thoroughly distribute plastic demands up the height of the building, are evident when reviewing results from the sweep and range scaling methods.

The upper floor plastic demands are most evident for the 20-story building subjected to the sweep-scaled motions. In contrast, the the range scaling method results in a mixture of some fundamental and higher modes, and the fundamental scaling method results in a primarily first-mode dominated plasticity distribution. The amount of plasticity experienced by these buildings was low, with average curvature ductility values ranging from about 1.3 to 2.0 (Table 5).

Table 5. Average rotation and ductility demands for beam members

Building	Method	$\theta_p$ ( $\times 10^{-3}$ rad)	$\mu_\theta$
8-story	Fundamental	1.69	1.55
	Range	2.57	1.84
	Sweep	1.83	1.62
12-story	Fundamental	2.02	1.62
	Range	1.55	1.48
	Sweep	1.4	1.44
20-story	Fundamental	3.03	1.99
	Range	0.77	1.25
	Sweep	0.83	1.27

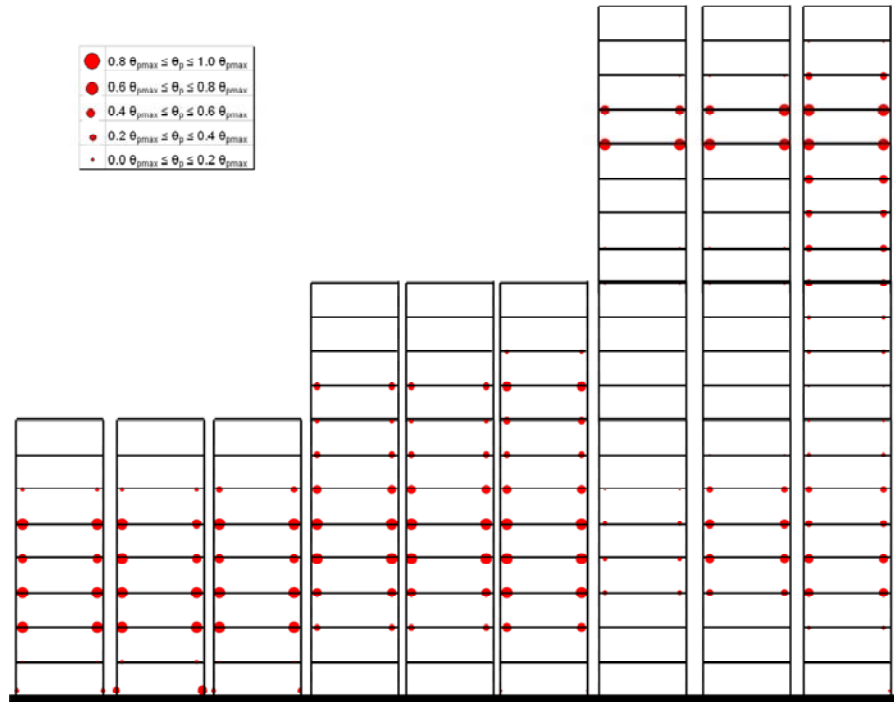


Figure 5. Average plasticity induced from time history analyses.

From left to right: Eight, twelve and twenty story buildings subjected to motions scaled according to the fundamental, range and sweep scaling methods.

### Conclusions

Three scaling methods are considered and nonlinear time history analyses of mid- and high-rise buildings conducted systematically using the same suite of earthquake motions. Nonlinear response of the buildings is evaluated in terms of plasticity distribution, floor level acceleration and uncorrelated acceleration amplification ratio distributions; and interstory drift distributions. It is consistently observed that scaling the input motions across a sweep of periods results in more robustly capturing the impact of higher mode response on the buildings nonlinear demands. Results from the sweep-based scaling approach diverge with response results estimated using a single modal period scaling approach, with the most pronounced divergence for taller buildings. Scaling the motions across minimally the first two predominant modes of vibration, which in this case captures 85% of the mass participation of the buildings; results in reasonably close comparison with the sweep-based scaling for all demand parameters evaluated and all buildings, with the exception of the tallest 20-story building.

Regardless of the scaling method considered, higher mode effects are observed for the mid- and high rise buildings considered, and when comparing the average maximum uncorrelated acceleration amplification factors to code-prescribed values, underestimation is consistently observed in the lower stories, while over-estimation is observed in the upper-most stories. An exception is the tallest building considered, where higher mode participation shifts the location of maximum acceleration demands towards the upper-most floor levels. These

demands can only be captured by scaling input earthquake motions across a period range which addresses the most significant modes of vibration of the building.

### Acknowledgements

This work was supported through funding provided by Hilti Corporation and NSF under grant number CMMI-0721399. Helpful suggestions of Professors Rob Dowell and Rolf Eligehausen and Dr. Matthew Hoehler are greatly appreciated. Opinions, findings, and conclusions expressed in this paper are those of the authors, and do not necessarily reflect those of the sponsoring agencies.

### References

- American Concrete Institute (2008) "Building code requirements for structural concrete." *ACI 318-08*, Farmington Hills, Michigan.
- ASCE 7-05. 2006. *Minimum Design Loads for Buildings and Other Structures*. American Society of Civil Engineers: Reston, VA.
- Bommer, J. J., and Acevedo, A. B. (2004) "The Use of Real Earthquake Accelerograms as Input to Dynamic Analysis." *Journal of Earthquake Engineering*, Vol. 8, No. 1, 43-91.
- Coleman, J., and Spacone, E. (2001) "Localization Issues in Force-Based Frame Elements." *Journal of Structural Engineering*. ASCE. Vol. 127, No.11, 1257-1265.
- Englekirk, R. E. (2003) *Seismic Design of Reinforced and Precast Concrete Buildings*. Wiley, New Jersey.
- Huang, Y.-N., A. S. Whittaker, N. Luco, and R. O. Hamburger (2009). "Selection and scaling of earthquake ground motions in support of performance-based design," *ASCE Journal of Structural Engineering*, In Press.
- ICC. (2006). *International building code 2006*. International Code Council, Falls Church, Va.
- Mander, J.B., Priestley, M. J. N., and Park, R. (1988a) "Theoretical Stress-Strain Model for Confined Concrete." *Journal of Structural Engineering*. ASCE. Vol. 114, No. 8, 1804-1826.
- Paulay, T. and Priestley, M. J. N. (1992). *Seismic design of reinforced concrete and masonry buildings*. John Wiley, and Sons Inc.
- PEER-NGA (2009) (Pacific Earthquake Engineering Research Center: NGA Database). <http://peer.berkeley.edu/nga/>
- Scott, M. H., and Fenves, G.L. (2006) "Plastic Hinge Integration Methods for Force-Based Beam-Column Elements." *Journal of Structural Engineering*. ASCE. Vol. 132, No. 2, 244-252
- Shome, N., and Cornell, C. A., 1998. Normalization and scaling accelerograms for nonlinear structural analysis, in *Proceedings of the Sixth U. S. Notional Conference on Earthquake Engineering*, CD-ROM, Seattle, WA
- Wood, R.L., Hutchinson, T.C., and Hoehler, M.S. (2009). *Cyclic Load and Crack Protocols for Anchored Nonstructural Components and Systems*. Structural Systems Research Project Report Series. SSRP 09/12. Department of Structural Engineering, University of California, San Diego. La Jolla, California.